CHINESE OPTICS LETTERS

Vol. 21, No. 2 | February 2023

Flexible omnidirectional reflective film for CO_2 laser protection

Wenling Chen (陈文玲)[1,†], Chao Liu (刘 超)[1,†], Yuqi Zou (邹郁祁)[1,†], Zhihe Ren (任志禾)[1], Yuanzhuo Xiang (向远卓)[1], Fanchao Meng (孟凡超)[2], Yinsheng Xu (许银生)[3], Chong Hou (侯 冲)[1,4], Sheng Liang (梁 生)[2], Lüyun Yang (杨旅云)[1], and Guangming Tao (陶光明)[1,5*]

[1] Wuhan National Laboratory for Optoelectronics and Sport and Health Initiative, Optical Valley Laboratory, Huazhong University of Science and Technology, Wuhan 430074, China

[2] Key Laboratory on Luminescence and Optical Information Technology of Ministry of Education, National Physical Experiment Teaching Demonstration Center, Department of Physics, School of Physical Science and Engineering, Beijing Jiaotong University, Beijing 100044, China

[3] State Key Laboratory of Silicate Materials for Architectures, Wuhan University of Technology, Wuhan 430070, China

[4] School of Optics and Electronic Information, Huazhong University of Science and Technology, Wuhan 430074, China

[5] State Key Laboratory of Material Processing and Die & Mould Technology, School of Materials Science and Engineering, Huazhong University of Science and Technology, Wuhan 430074, China

*Corresponding author: tao@hust.edu.cn

Received June 12, 2022 | Accepted August 12, 2022 | Posted Online September 13, 2022

In this Letter, we presented a flexible omnidirectional reflective film made of polymer substrates and multiple alternating layers of two chalcogenide glasses for full-angle CO_2 laser protection. The structure parameters of the device were simulated for theoretical prediction of best device structure. The reflector was fabricated by alternate thermal evaporation of two chalcogenide glasses with large refractive index contrast. The reflectivity was greater than 78% at 10.6 μm. The flexible reflective film can provide an effective solution for full-angle CO_2 laser protection of the moving targets, such as laser operators and mobile optical components, with potential applications for wearable laser protective clothing.

Keywords: omnidirectional reflective film; flexible reflector; CO_2 laser protection; chalcogenide glass.
DOI: 10.3788/COL202321.022201

1. Introduction

The CO_2 laser is widely utilized in industrial manufacture and clinical medicine[1] for its non-contact nature, high precision, high energy, and power tunability. With a special working window in the 9–11 μm wavelength range, in which light is strongly absorbed by biological tissues components, such as hydroxyapatite and water[2], the CO_2 laser could efficiently ablate both hard and soft tissues[3], and thereby it is widely used in surgical clinical treatment, such as otolaryngology[4] and neurosurgery[5]. However, the widespread use of high-energy CO_2 lasers creates safety hazards for exposed humans. Once fault oriented, CO_2 laser power of more than 5 W on the cornea and skin can cause loss of vision[6,7] and burns[6,8], respectively. Moreover, CO_2 lasers have been extensively employed in the material processing industry[9] due to the CO_2 laser being strongly absorbed by materials such as paper, wood, plastics, glass, stone, and different composite materials products[10,11]. Hence, high-energy CO_2 laser irradiation on optical components can inflict damage on optical performance[12]. At present, common protective equipment for CO_2 laser irradiation is mainly based on reflective lenses of rigid glass substrate[13]. This device is with high cost, lacking of lightweight feel, and limited pinpoint accuracy and accessibility for operators. In practical applications, there is a need to enhance the flexibility and maneuverability of protective equipment to accommodate the requirements for the protection of movable joints and mobile optical components[13]. Optical metamaterials based on one-dimensional photonic crystals show promise in optical field regulation with scalability[14–16]. The photonic bandgap structure in thin sheet (thickness: several tens to hundreds of micrometers)[17] can achieve high reflectivity at a specific wavelength ($R \sim 99\%$). The structural design using the mid-infrared photonic band on a polymer substrate can provide enhanced film flexibility and reflectivity to extend the protection range for wearable needs[18–20].

Chalcogenide glasses (ChGs) are an ideal material with excellent mid-infrared transmission performance (at least in the 9–11 μm window), low cost, and stable manufacturing capabilities and are the only glassy materials that can cover the transmission

window in the 3–12 μm wavelength range with more stable chemical properties, mature production processes, and lower costs than crystalline materials[21,22]. In addition, ChGs have the advantages of adjustable components and precision moulding, and the optical refractive index can be adjusted in the range of 2–4 by component control. In 2009, Kohoutek *et al.*[23] prepared a near-infrared one-dimensional photonic crystal omnidirectional reflector based on ChGs with 98.8% normal incidence stopband of the reflector at 1.55 μm.

In this paper, we reported a flexible omnidirectional reflective film based on a periodic photonic structure. The parameters of the laser wavelength, incident angle, transverse electrical (TE) or magnetic (TM) mode, and film period thickness and number were changed to simulate the theoretical prediction of the best device structure. The reflector was fabricated by alternating thermal evaporation of two ChGs ($Ge_{20}As_{20}Se_{18}Te_{42}$ and $As_{40}S_{60}$) with large refractive index contrast and excellent thermal stability[24]. The optical properties of the resulting reflector were characterized using Fourier transform infrared spectrometer (FTIR) to demonstrate the discrepancy between theoretical predictions and experiments. The results show that our reflector can achieve full-angle (0°–90°) CO_2 laser protection for the targets in locomotion.

2. Numerical Simulation

2.1. Flexible high-reflection film structure model and photonic bandgap calculation

The structure of one-dimensional photonic crystal reflective film is depicted in Fig. 1(a), where d_s, d_h, and d_l are the layer thicknesses, and n_s, n_h, and n_l are the refractive indices of the polymer layer, high-refractive-index layer, and low-refractive-index layer, respectively.

In theoretical simulations, for the purpose of omnidirectional laser reflection, two materials with large refractive index difference are required to achieve photonic band gap in the CO_2 laser operating band. In addition, both materials are required to have a long infrared cut-off wavelength (at least 12 μm). Therefore, two ChGs, $Ge_{20}As_{20}Se_{18}Te_{42}$ ($n = 3.068$ at 10 μm)[25] and $As_{40}S_{60}$ ($n = 2.37$ at 10 μm)[26], are chosen as the high-refractive-index and low-refractive-index materials, respectively, which are stable glasses with excellent thermal stability, glass forming ability, and large adjustable refractive index range. The thicknesses are taken according to the quarter wave stack condition, $d_h = \lambda_0/4n_h$ and $d_l = \lambda_0/4n_l$. Taking the CO_2 laser wavelength as the central wavelength ($\lambda_0 = 10.6\,\mu m$), the film thicknesses can be determined as $d_h = 0.8638\,\mu m$ and $d_l = 1.1181\,\mu m$, respectively. The 45 μm polyphenylene sulfone resins (PPSU) polymer film is derived as a substrate to provide flexibility to the omnidirectional reflector. Considering that the ChGs are fragile and easy to be oxidized, a polymethyl methacrylate (PMMA) polymer film layer is added on the surface as a protective layer. According to the designed structure, the band diagram of the photonic crystal was obtained using a standard transfer matrix method, as shown in Fig. 1(b), which allows for the analysis of propagating and evanescent modes in the structure, corresponding to a real or imaginary Bloch wave number solution[27,28]. The omnidirectional band of this structure spans from 10 μm to 10.7 μm defined by the band edges ω_l and ω_h.

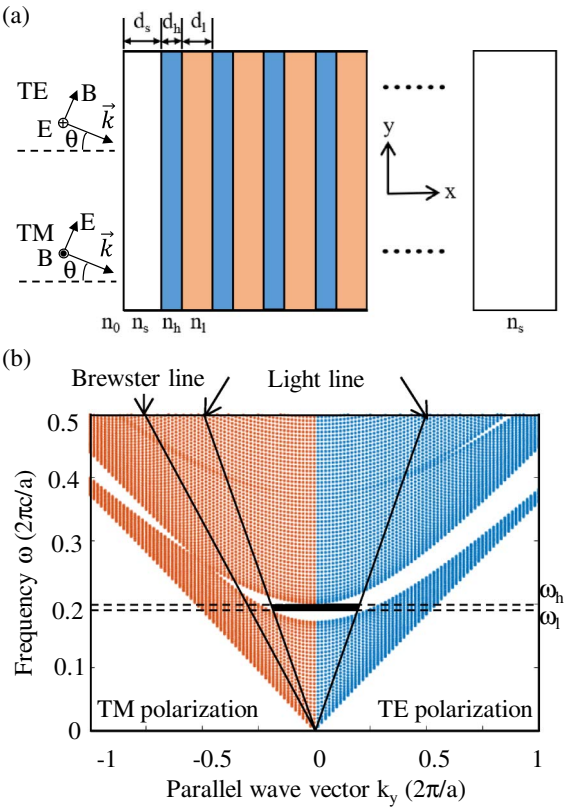

Fig. 1. Structure model and photonic bandgap. (a) Schematic of flexible reflective film; (b) photonic bandgap diagram for a one-dimensional photonic crystal.

2.2. Structural parameter simulation

The reflection properties of one-dimensional photonic crystal structures under different structural parameters were investigated using COMSOL 6.0 based on the transmission matrix method. As shown in Figs. 2(a) and 2(b), under the condition of normal incidence, no matter whether the PMMA coating is added or not, with the increase of the number of cycles (N_c), the reflectance at the center wavelength gradually increases (ultimately more than 95%), and the bandgap width gradually decreases. When the N_c reaches eight, the reflectivity and bandgap width do not change significantly with further increase of N_c. The early study results show that polymer film coated with 30 μm glass material is still bendable and robust, which means that when a 5 μm PMMA coating is added to the surface layer the photonic bandgap width decreases significantly for low N_c structures, but, when the N_c increases above eight, the effect is negligible.

The reflectances of TE and TM polarizations with PMMA coating at 0°, 15°, 30°, 45°, 60°, 70°, and 80° angles are

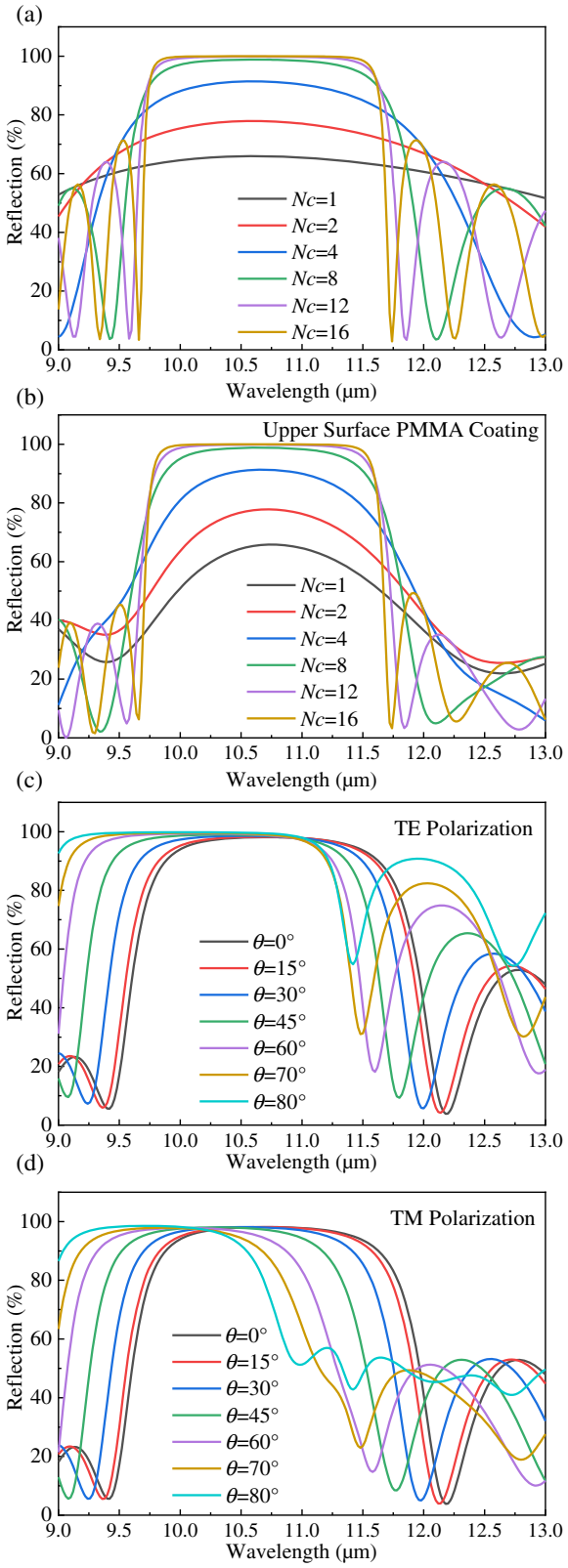

Fig. 2. Structural parameter simulation. (a) Reflectance spectra of the structure without coating at different periods; (b) reflectance spectra of the structure with upper surface PMMA coating at different periods; (c) and (d) reflectance ranges for TE and TM polarization modes at different incident angles with upper surface PMMA coating.

represented in Figs. 2(c) and 2(d). It can be found that the effective optical thickness of the photonic crystal structure film gradually decreases when the incident angle increases, causing the energy bands of TE and TM polarized waves to shift toward high frequencies. For the TE mode, both the forbidden band width and the central wavelength reflectance increase with the incident angle, while the opposite is true for the TM mode. However, the reflectivity can still reach above 87% in the 9.8–10.6 μm band.

3. Experiment

In this experiment, high-purity $As_{40}S_{60}$ and $Ge_{20}As_{20}Se_{18}Te_{42}$ were prepared by the melt-quenching method[29,30]. The one-dimensional photonic crystal structure was prepared by the vacuum thermal evaporation technique. The evaporation rates and film thicknesses were measured by a quartz crystal monitor. The $As_{40}S_{60}$ film (evaporating temperature ~370°C, residual pressure $\sim 8 \times 10^{-4}$ Pa, deposition rate ~4–6 Å/s) as the low-refractive-index component and the $Ge_{20}As_{20}Se_{18}Te_{42}$ film (evaporating temperature ~460°C, residual pressure $\sim 1 \times 10^{-3}$ Pa, deposition rate ~4–6 Å/s) as high-refractive-index components were alternately deposited on cleaned PPSU polymer films with a thickness of 45 μm to obtain a one-dimensional photonic crystal reflective film. Surface polymer PMMA film was prepared using a spin-coating method from the solution of N,N-dimethylformamide. Polymer film was coated by spinning for 30 s at a spin speed of 2000 r/min and heated in the vacuum furnace at 60°C and 5 Pa.

The principle of vacuum thermal evaporation and spin coating is shown in Fig. 3(a), and the obtained flexible one-dimensional photonic crystal reflective film is shown in Fig. 3(b). The reflective film exhibits high flexibility compared

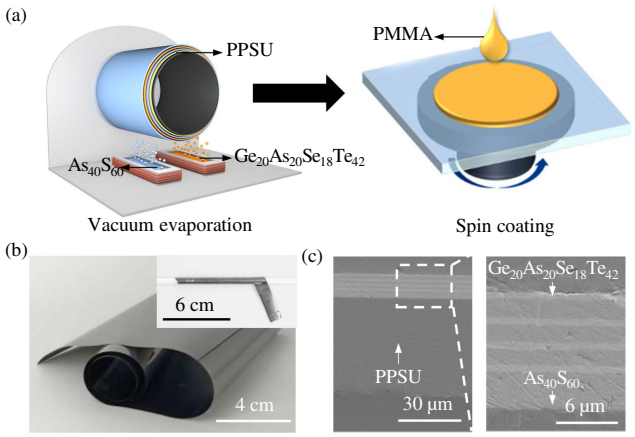

Fig. 3. Experimental principle and device diagram. (a) The principle of vacuum thermal evaporation and solution spin coating; (b) the obtained flexible one-dimensional photonic crystal reflective film (inset shows a flexible reflective film being wound on a 5-mm-diameter glass rod); (c) SEM cross-sectional images of cleaved chalcogenide reflector show periodic alternation of films in the multilayers.

to other reflectors with rigid substrates and can be bent at will with a bending radius of less than 2.5 mm. Scanning electron microscopy (SEM) was used to capture the cross-sectional images of the omnidirectional reflective film to show the periodicity and interface quality of the reflector obtained by vacuum thermal evaporation. The mirrors were polished before the images were recorded. The normal incidence reflectivity spectra of the prepared flexible reflector were recorded in the range of 7–14 μm using the FTIR, and the reflectivity spectra of the flexible reflector under the incident angles of 0°, 30°, 45°, and 60° were measured by using a self-built test platform based on FTIR.

4. Results and Discussion

The SEM cross-section image of the prepared four-period omnidirectional reflectivity film, Fig. 3(c), shows the film sequence. The bottom layer is the PPSU substrate, on the top of which is the $Ge_{20}As_{20}Se_{18}Te_{42}$ and $As_{40}S_{60}$ glass with alternating structures. As shown in the figure, the upper three periodic structures have uniform periodic thicknesses with an average thickness of 1.93 μm, which is consistent with the expected results. The lowermost layer has a relatively higher cycle thickness, mainly due to the stress effect between the glass and the polymer.

Figure 4(a) illustrates the normal incidence reflection spectra of the prepared flexible reflective films with different periods and added polymer layers in the range of 7–14 μm, which is in complete agreement with the simulation results. With the increase of N_c, the reflectivity of the photonic bandgap structure gradually increases, and the photonic bandgap gradually increases. Meanwhile, there is a certain deviation between the periodic thickness of the prepared film and the thickness ratio of the high- and low-refractive-index glass compared with the simulation results, which causes the central wavelength of the photonic bandgap to move to the high-frequency direction, which is consistent with the simulation results. The fabricated four-period flexible reflector was studied by the FTIR; it indicated that the central wavelength was 10.2 μm, and the reflectivity was greater than 78% at 10.6 μm, which is close to the expected result.

The reflection spectra of the four-period reflective film at different incident angles, namely 0°, 30°, 45°, and 60°, were measured by FTIR, and the results are shown in Fig. 4(b). We observed very good agreement between the calculated and measured reflectance spectra. With the increase of the incident angle, the central wavelength gradually decreases, the maximum reflectivity at the central wavelength also decreases, and the bandgap width decreases, mainly because the effective optical thickness of the film layer of the photonic crystal structure gradually decreases. The reasons for the deviation in Figs. 4(a) and 4(b) include the intrinsic impurity absorption of ChGs materials and the absorption of external impurities introduced during the glass processing (e.g., glass grinding).

Figure 4(c) shows the reflection spectra of the one-dimensional photonic crystal reflective films with different period thicknesses, both of which are four periods, and the central wavelengths are 10.1 μm ($d_h = 0.85$ μm and $d_l = 1.09$ μm) and 8.5 μm ($d_h = 0.71$ μm and $d_l = 0.91$ μm), respectively. The shift of the central wavelength according to period thickness is attributed to the photonic bandgap shifting. By changing the period thickness, the photonic bandgap can be shifted in the wavelength of 1–12 μm.

5. Conclusion

In conclusion, we designed, fabricated, and characterized a flexible omnidirectional reflective film for full-angle CO_2 laser protection of exposed operators and locomotive optical components. The reflector, composed of four periods of $Ge_{20}As_{20}Se_{18}Te_{42}$ and $As_{40}S_{60}$ alternating layers, exhibits 78% reflectance at 10.6 μm, which was consistent with the theoretical simulation. With the increasing number of alternating periods, the highest reflectivity will reach more than 95%. In addition, based on the high transparency of ChGs in the infrared window,

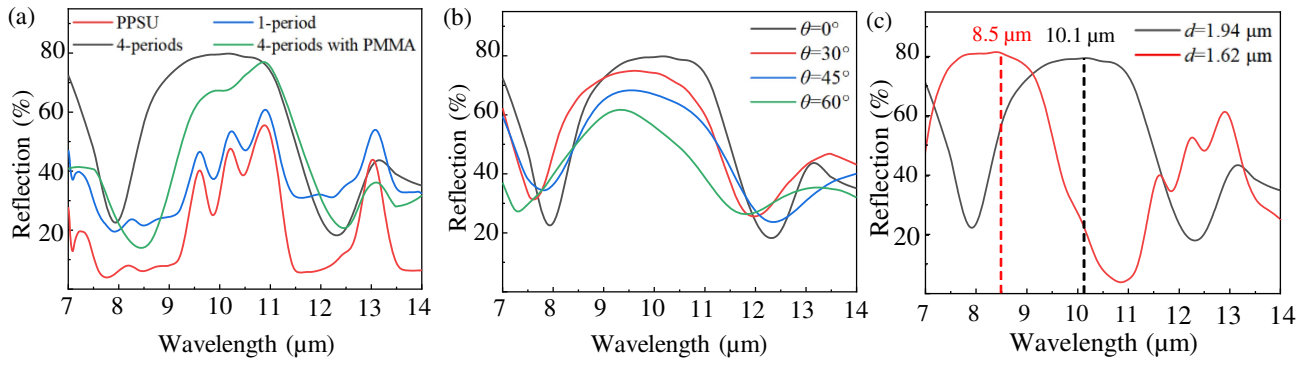

Fig. 4. Reflection spectra of one-dimensional photonic crystals under different conditions. (a) The reflection spectra of prepared chalcogenide multilayers with different periods and added polymer layers, namely PPSU (red), one period (blue), four periods (black), and four periods with upper surface PMMA coating (green); (b) the reflection spectra of the prepared four-period chalcogenide multilayers at different incident angles, namely 0° (black), 30° (red), 45° (blue), and 60° (green); (c) the reflection spectra of prepared chalcogenide multilayers with different period thicknesses, d is 1.94 μm (black) and 1.62 μm (red) corresponding to λ_0 of 10.1 μm and 8.5 μm.

the band gap of the multi-layer film can be adjusted in the range of 1–12 μm by changing the period thickness. Flexible omnidirectional dielectric mirror fibers also can be designed as woven fabrics for radiation barriers.

Acknowledgement

This work was supported by the National Natural Science Foundation of China (No. 61875064). The authors are grateful for the assistance from the Analytical and Testing Center of Huazhong University of Science and Technology (HUST).

References

1. E. Khalkhal, M. Rezaei-Tavirani, M. R. Zali, and Z. Akbari, "The evaluation of laser application in surgery: a review article," J. Lasers Med. Sci. **10**, S104 (2019).
2. H. Arslan and B. Pehlivanoz, "Effect of purification, dehydration, and coagulation processes on the optical parameters of biological tissues," Chin. Opt. Lett. **19**, 011701 (2021).
3. M. Shurgalin and C. Anastassiou, "A new modality for minimally invasive CO_2 laser surgery: flexible hollow-core photonic bandgap fibers," Biomed. Instrum. Technol. **42**, 318 (2008).
4. S. Mihashi, G. J. Jako, J. Incze, M. S. Strong, and C. W. Vaughan, "Laser surgery in otolaryngology: interaction of CO_2 laser and soft tissue," Ann. N. Y. Acad. Sci. **267**, 263 (1976).
5. R. W. Ryan, T. Wolf, R. F. Spetzler, Y. Fink, and M. C. Preul, "Application of a flexible CO_2 laser fiber for neurosurgery: laser-tissue interactions: laboratory investigation," J. Neurosurg. **112**, 434 (2010).
6. D. J. Fader and D. Ratner, "Principles of CO_2/erbium laser safety," Dermatol. Surg. **26**, 235 (2000).
7. C. Daggett, A. Daggett, E. McBurney, and A. Murina, "Laser safety: the need for protocols," Cutis **106**, 87 (2020).
8. R. J. Rockwell, "Laser accidents: reviewing thirty years of incidents: what are the concerns-old and new?" J. Laser Appl. **6**, 203 (1994).
9. W. Rath and C. Brettschneider, "Industrial laser materials processing: a review of the origin, current status and an outlook," Laser Tech. J. **11**, 23 (2014).
10. C. Tan, L. Zhao, M. Chen, J. Cheng, Z. Yin, Q. Liu, H. Yang, and W. Liao, "Combined studies of surface evolution and crack healing for the suppression of negative factors during CO_2 laser repairing of fused silica," Chin. Opt. Lett. **19**, 041402 (2021).
11. J. Huang, Y. Lu, Z. Wu, Y. Xie, C. He, and J. Wu, "Infrared broadband nonlinear optical limiting technology based on stimulated Brillouin scattering in As_2Se_3 fiber," Chin. Opt. Lett. **20**, 031902 (2022).
12. D. Ristau, M. Jupé, and K. Starke, "Laser damage thresholds of optical coatings," Thin Solid Films **518**, 1607 (2009).
13. G. Ritt, S. Dengler, and B. Eberle, "Protection of optical systems against laser radiation," Proc. SPIE **7481**, 74810U (2009).
14. V. P. Stinson, S. Park, M. McLamb, G. Boreman, and T. Hofmann, "Photonic crystals with a defect fabricated by two-photon polymerization for the infrared spectral range," Optics **2**, 284 (2021).
15. A. L. Goyal and A. Kumar, "Recent advances and progresses in photonic devices for passive radiative cooling application: a review," J. Nanophotonics **14**, 030901 (2020).
16. Á. Blanco and C. López, "Photonic crystals: fundamentals and application," Annu. Rev. Nano Res. **1**, 81 (2006).
17. D. N. Chigrin, A. V. Lavrinenko, D. A. Yarotsky, and S. V. Gaponenko, "All-dielectric one-dimensional periodic structures for total omnidirectional reflection and partial spontaneous emission control," J. Light. Technol. **17**, 2018 (1999).
18. Y. Yue and J. P. Gong, "Tunable one-dimensional photonic crystals from soft materials," J. Photochem. Photobiol. C **23**, 45 (2015).
19. L. Li, H. Lin, S. Qiao, Y. Zou, S. Danto, K. Richardson, J. D. Musgraves, N. Lu, and J. Hu, "Integrated flexible chalcogenide glass photonic devices," Nat. Photonics **8**, 643 (2014).
20. W. Yan, C. Dong, Y. Xiang, S. Jiang, A. Leber, G. Loke, W. Xu, C. Hou, S. Zhou, M. Chen, R. Hu, P. P. Shum, L. Wei, X. Jia, F. Sorin, X. Tao, and G. Tao, "Thermally drawn advanced functional fibers: new frontier of flexible electronics," Mater. Today **35**, 168 (2020).
21. C. R. Petersen, M. B. Lotz, C. Markos, G. Woyessa, D. Furniss, A. B. Seddon, R. J. Taboryski, and O. Bang, "Thermo-mechanical dynamics of nanoimprinting anti-reflective structures onto small-core mid-IR chalcogenide fibers," Chin. Opt. Lett. **19**, 030603 (2021).
22. G. Tao, H. Ebendorff-Heidepriem, A. M. Stolyarov, S. Danto, J. V. Badding, Y. Fink, J. Ballato, and A. F. Abouraddy, "Infrared fibers," Adv. Opt. Photonics **7**, 379 (2015).
23. T. Kohoutek, J. Orava, J. Prikryl, J. Mistrik, T. Wagner, and M. Frumar, "Near infrared quazi-omnidirectional reflector in chalcogenide glasses," Opt. Mater. **32**, 154 (2009).
24. J. A. Frantz, A. Clabeau, J. D. Myers, R. Y. Bekele, V. Q. Nguyen, and J. S. Sanghera, "Thermal tuning of arsenic selenide glass thin films and devices," Opt. Express **28**, 34744 (2020).
25. G. Tao, S. Shabahang, H. Ren, F. Khalilzadeh-Rezaie, R. E. Peale, Z. Yang, X. Wang, and A. F. Abouraddy, "Robust multimaterial tellurium-based chalcogenide glass fibers for mid-wave and long-wave infrared transmission," Opt. Lett. **39**, 4009 (2014).
26. Y. Sun, S. Dai, P. Zhang, X. Wang, Y. Xu, Z. Liu, F. Chen, Y. Wu, Y. Zhang, R. Wang, and G. Tao, "Fabrication and characterization of multimaterial chalcogenide glass fiber tapers with high numerical apertures," Opt. Express **23**, 23472 (2015).
27. Y. Fink, N. Winn Joshua, S. Fan, C. Chen, J. Michel, J. D. Joannopoulos, and E. L. Thomas, "A dielectric omnidirectional reflector," Science **282**, 1679 (1998).
28. J. N. Winn, Y. Fink, S. Fan, and J. D. Joannopoulos, "Omnidirectional reflection from a one-dimensional photonic crystal," Opt. Lett. **23**, 1573 (1998).
29. G. Tao, S. Shabahang, E.-H. Banaei, J. J. Kaufman, and A. F. Abouraddy, "Multimaterial preform coextrusion for robust chalcogenide optical fibers and tapers," Opt. Lett. **37**, 2751 (2012).
30. B. Zhang, C. Zhai, S. Qi, W. Guo, Z. Yang, A. Yang, X. Gai, Y. Yu, R. Wang, D. Tang, G. Tao, and B. Luther-Davies, "High-resolution chalcogenide fiber bundles for infrared imaging," Opt. Lett. **40**, 4384 (2015).